Near-Surface Snow Particle Dynamics from Particle Tracking Velocimetry and Turbulence Measurements during Alpine Blowing Snow Storms

Nikolas O. Aksamit[1], John W. Pomeroy

[1]Centre for Hydrology, University of Saskatchewan, Saskatoon, S7N 5C8, Canada

Correspondence to: Nikolas O. Aksamit (n.aksamit@usask.ca)

Abstract. Many blowing snow conceptual and predictive models have been based on simplified two-phase flow dynamics derived from time-averaged observations of bulk flow conditions in blowing snow storms. Measurements from the first outdoor application of Particle Tracking Velocimetry (PTV) of near-surface blowing snow yields new information on mechanisms for blowing snow initiation, entrainment, and rebound, whilst also confirming some findings from wind tunnel observations. Blowing snow particle movement is influenced by complex surface flow dynamics, including saltation development from creep that has not previously been measured for snow. Comparisons with 3D atmospheric turbulence measurements show that blowing snow particle motion immediately above the snow surface responds strongly to high frequency turbulent motions. Momentum exchange from wind to the dense near-surface particle-laden flow appears significant and makes an important contribution to blowing snow mass flux and saltation initiation dynamics. The more complete and accurate description of near-surface snow particle motions observable using PTV may prove useful for improving blowing snow model realism and accuracy.

1 Introduction

Wind transport of snow influences the variability of alpine summer runoff (*Pomeroy et al.*, 2012; *Winstral et al.,* 2013), is a large contributor to the growth or ablation of small mountain glaciers (*Dyunin and Kotlyakov*, 1980), and can contribute snow loading to avalanche prone areas (*Schweizer et al.*, 2003). Time-averaged blowing snow field measurements often present an oversimplified view of a highly variable and unsteady natural phenomenon. Physical snow trap mechanisms only provide mass flux averages over prolonged collection periods (*Budd et al.*, 1966). Snow particle counters only recently began providing point measurements of particle speed (*Nishimura et al.,* 2014) along with particle size and number flux values (*Schmidt*, 1984; *Brown and Pomeroy*, 1989; *Kinar and Pomeroy,* 2015). Snow traps and particle counters can neither measure the mechanisms of transport initiation nor provide continuous vertical profiles of particle concentration or transport. Yet, most current blowing snow model development has been informed from time-averaged measurements from such devices. Accordingly, simple models of blowing snow persist in the literature that do not contain self-consistent wind-snow momentum balances, as demonstrated by *Andreotti* (2004). As well, there is a current as a lack of detailed measurements of particle-surface interactions in natural conditions.

Recent progress in blowing snow research has been accelerated by novel applications of high-speed imaging systems. *Kobayashi* (1972) pioneered blowing snow recordings with outdoor, 1/8-second shutter speed images. This was the first visual evidence of particle mechanics in the snow saltation layer and was extremely informative in the development of saltation theory (*Pomeroy and Gray*, 1995), but the photographs consisted of blurred snow particle streaks or were saturated

5   with particles, disguising individual particle motions. More recently, *Gordon and Taylor* (2009) designed a novel and effective halogen backlit camera system to effectively obtain particle size and shape parameters in the Arctic, but were limited to an imaging area on the order of 9 mm^2. In a further study, *Gordon et al.* (2009) modified this technique to image an area of 124 mm x 101 mm with a black and white binarization algorithm to obtain continuous particle density profiles. Unfortunately, particle velocity measurements were unavailable from either study.

10   In laboratories, several wind tunnel studies have examined drifting snow with Particle Image Velocimetry (PIV) (*Lu et al.,* 2012; *Tominaga et al.*, 2012), shadowgraphy (*Gromke et al*., 2014) and shadowgraphic Particle Tracking Velocimetry (PTV) (*Groot Zwaaftink et al.*, 2014), providing valuable insights into saltating snow velocity distributions, average relative wind and saltating snow velocities, particle size distributions and qualitative comparisons to Large Eddy Simulation driven transport. Blowing snow transport model development continues to address small-scale variability (e.g. *Nemoto and*

15   *Nishimura*, 2004; *Groot Zwaaftink et al*., 2014), and requires advanced measurement techniques to understand the physics driving such multi-scale heterogeneities as well as evaluate the uncertainties and assumptions inherent in proposed models.

Of the multitude of blowing snow models that have been developed, many implement components of earlier aeolian saltation or initiation models, e.g. the work of *Bagnold* (1941), *Owen* (1964), *Schmidt* (1980), *Pomeroy and Gray* (1990), and *Nishimura and Hunt* (2000). In what follows, effort has been made to refer only to the original work containing the model

20   component or measurement campaign under discussion, but comments generally apply to all derivatives. Following the work of *Bagnold* (1941), current theory often represents blowing snow in two layers, saltation and suspension, with a neglected and poorly understood creep mechanism at the lower boundary of saltation (*Pomeroy and Gray*, 1990; *Nishimura and Hunt*, 2000; *Doorschot and Lehning*, 2002). Once the wind surpasses a transport threshold velocity, saltating particles follow ballistic trajectories, and rebound off the surface, rising no higher than 10 cm. As wind speeds increase, saltating particles

25   become suspended by turbulence and disperse upwards. Closely following wind streamlines, suspended particles rarely encounter the ground (*Pomeroy and Male*, 1992; *Bintanja*, 2000).

The two most commonly modeled modes of saltation initiation are *aerodynamic lift*, the direct drag induced ejections of grains, and *splash*, the ejection of grains by rebounding saltating particles (*Doorschot and Lehning*, 2002, *McElwaine et al.,* 2004). However, there are substantial disagreements about these mechanisms; *Schmidt* (1986) calculated that direct

30   aerodynamic lift was not possible under average flow conditions over a level snow surface due to strong snow particle bonding. *Doorschot et al.* (2004) argued the fragile dendritic snow in their study resulted in aerodynamic lift dominance. *Pomeroy* (1988) was unable to identify different threshold wind speeds for either aerodynamic lift or particle splash to dominate. It is likely that both mechanisms are possible and that the prevalent mechanism depends on the wind conditions and snow surface structure and cohesion. There is a growing pool of blowing snow models parameterizing these two

initiation mechanisms, including the work of *Doorschot and Lehning* (2002), *Nemoto and Nishimura* (2004) and *Groot Zwaaftink et al.* (2014), all adapting the blowing sand initiation model of *Anderson and Haff* (1991) through wind tunnel measurements.

In contrast to representing saltation as a layer of particles moving with uniform trajectories (i.e. Owen, 1964) as is common in snow saltation studies (*Pomeroy and Gray*, 1990; *Tabler*, 1991; *Doorschot and Lehning*, 2002), recent wind tunnel studies and numerical simulations of wind transport of sand have shown the benefit of representing saltation with continuous grain velocity distribution functions (*Creysells et al.,* 2009; *Ho et al.,* 2011, 2012, 2014). From these observations, two populations of saltating particles are distinguishable by kinetic energy rather than by physical properties such as grain size. High-energy particles have higher and longer trajectories that are influenced by changes in wind strength. However, these particles only constitute the long tails of velocity distribution functions (*Ho et al.,* 2012). The bulk of sand saltation observed in these studies consists of low-energy splashed 'ejecta' and tractating (bed transport) grains undergoing very short hops. These grains generate the majority of mass flux and govern the mean properties of equilibrium saltation (*Ho et al.,* 2014).

As saltation develops, transport mechanics evolve. For instance, in sand, saltation and creep transport modes are often coupled when saltation begins (*Willets et al.,* 1991): as low-energy surface particles accelerate, they begin feeding upper regions of saltation. Allowing variability of motion in blowing snow saltation models permits consideration of additional mechanisms of saltation initiation and momentum transfer to the snow surface.

It remains unknown how well recent advances in conceptualization of blowing sand transport can improve descriptions of blowing snow because detailed observations of outdoor blowing snow particle transport processes near the snow surface have not been conducted. Perhaps due to this, current theories of snow saltation are inconsistent with each other and conceptualize a limited range of snow motions and initiation mechanisms. To improve the physical theory of blowing snow initiation and transport, this study demonstrates PTV as a tool for measuring short timescale blowing snow surface motions in an outdoor environment. The objectives of this study are to examine the mechanics of snow particle motion initiation, the detailed interactions between wind speed fluctuations and snow particle dynamics, and the role of turbulent burst mechanisms that are common in mountain environments in generating shear stress to modify snow saltation. In doing so, the potential for adapting a continuum sand transport model for describing snow saltation particle motions is assessed.

2 Methods

Fieldwork was conducted during blowing snow events from February to April 2015 at the Fortress Mountain Snow Laboratory (FMSL), Kananaskis Valley, Alberta, Canada. FMSL receives at least 800 mm water equivalent of snowfall each winter, can sustain wind speeds exceeding 35 m s^{-1} and is home to several well-instrumented high-altitude, wind-swept observation sites. The blowing snow site (2000 m.a.s.l.) is located in an open base area of the Fortress Mountain ski area (Figure 1). The area was lightly used, allowing for a 350 m upwind fetch of undisturbed open snowfield, with the foot of a moderate ridge flanking the west 200 m away. The ground was snow-covered and shrub vegetation buried for the duration of

the experiment with snow depths fluctuating from 70 to 120 cm. Two Campbell Scientific CSAT3 three-dimensional ultrasonic anemometers positioned at varying heights (typically 40 and 200 cm) on a single mast measured wind speed at 50 Hz in three axes.

5   The unique aspect of this experiment was the implementation of laser-illuminated high-speed videography for outdoor nighttime snow particle tracking observations. A portable rigid frame equipped with a Megaspeed MS85K high-speed camera and a 445 nm wavelength 1.5-Watt continuous-wave laser was situated on the snow surface, typically 1 m downwind from the anemometer mast. The frame was positioned on the snow surface allowing the camera a perpendicular 30 mm x 140 mm view of the flow of saltating snow. Laser light was projected through a cylindrical lens to create a 2 mm wide plane orthogonal to both the snow surface and the view of the camera (Fig. 1). The light plane illuminated a 2D projection of

10   saltating snow particles. This allowed recordings in the lowest 10 cm of the atmosphere, with minimal foreground shadowing and no background reflection.

Particle Tracking Velocimetry (PTV) measurements were calculated by DaVis 8 (LaVision) software and estimated individual snow particle velocities using tracking algorithms that match discrete particles in subsequent frames imaged by the high-speed camera. Particle velocimetry techniques are normally used for wind tunnel studies (e.g. *Zhang et al.,* 2007;

15   *Creyssels et al.*, 2009; *Ho et al.,* 2011, 2012; *Lu et al.,* 2012; *Tominaga et al.,* 2012; *Groot-Zwaaftink et al.*, 2014), with few applications, in any discipline, in an outdoor setting (e.g. *Morris et al.,* 2007; *Zhu et al.,* 2007; *Rosi et al.,* 2014; *Toloui et al.,* 2014). This is the first known application of PTV for boundary-layer blowing snow studies in a natural environment.

The high-speed saltation recordings provide a great degree of visual distinction of surface particle motion and the use of 2D laser illumination minimizes particle overlap (e.g. *Kobayashi*, 1972). As the camera was focused close to the snow surface,

20   hundreds of thousands of rebound and splash events were recorded over the winter field season. In addition to PTV, video was later reviewed with playback reduced 100 times, providing qualitative insight to the mechanics of near-surface saltating particle motion and bed interactions.

Figure 2 displays an example of velocity vectors calculated from 1 second of 23 March 2015, recording #3. The stationary snow surface has been masked out. The dashed black line indicates the height (h_0) of the upper limit of particles whose

25   velocities are heavily influenced by surface microtopography and contribute uncharacteristic velocity profile statistics (analogous marks exist in Figure 3). PTV vector fields such as this were used to calculate vertical profiles of mean projected horizontal particle velocity u_p, (Fig. 3a-f) and particle number flux concentrations F_z, (Fig. 3g). The PTV region of interest was vertically partitioned into horizontal slices following a log-scale. This allowed particle bin sizes to remain consistent for velocity averages as particle number density exponentially decreased with height. In Fig. 3, the height of surface

30   microtopography varies as recordings were made over hours of active erosion and deposition, changing the surface structure. The improved realism afforded by PTV over a natural snowpack in the atmospheric boundary layer (ABL) is counterbalanced by increased difficulty in obtaining valuable data from this methodology and from sonic anemometry during blowing snow storms. Concurrent ultrasonic wind speed measurements sometimes included spikes, "NaN" readings or were flagged for skewness/kurtosis (*Vickers and Marht*, 1997); these video recordings were used only for qualitative

comparison. Spanwise fluctuations in wind caused snow particles to travel transverse to the plane of light, and the streamwise wind direction usually varied at the blowing snow site over the course of an evening's observations. PTV relies on particles to remain in the plane of light for illumination and tracking through multiple frames. While the frame could be adjusted for slow variations in wind direction, directional variations during wind gusts were a significant complication.

5   To reduce particle mismatch errors and improve velocity calculation accuracy, initial visual quality controls were implemented, discarding video that contained particles obviously moving transverse to the plane of light. Upon processing, individual particles were required to be evident in at least four frames; this reduced the number of video frames providing PTV vector fields from 551,000 to 190,000, resulting in 560,000 snow particle velocity vectors calculated for 165 seconds of real time recording. The camera depth of field and light plane thickness limited out-of-plane particle velocity components to

10    $\pm 0.5 ms^{-1}$.

Further uncertainty derives from the limited ability of PTV software to match individual snow particles at high wind speeds (> 9 m s^{-1} at 40 cm height). The particle matching interrogation area becomes larger as wind speeds increase and particles travel further from one frame to the next. This exponentially increases the number of particles that may be incorrectly matched. To address this problem, a single-threshold black and white binarization technique (*Otsu*, 1979) was used to obtain

15   measurements of the snow particle pixel area in individual frames. The pixel area measurements are not affected by transverse particle motion or tracking algorithm limitations. Binarization estimates were in sufficient qualitative agreement with concentration profiles generated by PTV to lend confidence to the measurements of particle trajectories. PTV measurements in exceptionally high wind speeds (> 10 m s^{-1}) were not possible because the laser light became blocked by particles. Therefore, the dataset used in this analysis is focused on observations taken during relatively low mean wind

20   speeds for blowing snow; these sometimes included periods of intermittent turbulent bursts and intermittent snow transport.

3 Results

Examination of data calculated from 23 March, 2015 demonstrates the value of PTV measurements over varying wind speeds during a period without significant changes in saltating grain shape, type, or size. Following the designations of the International Classification for Seasonal Snow on the Ground (*Fierz et al.,* 2009), saltating snow consisted of spherical

25   graupel grains (mean diameter 413 μm) with many reaching 1000 μm in diameter. The bed was composed of 5 cm of fresh loose grains that had fallen the day of recording with a hand hardness index of 1 (Very Soft/Fist) over a supportive melt-freeze crust with no foot penetration. Snow transport was highly intermittent, implying wind speeds were near threshold conditions. The small initial surface cohesion did not appear to be increased by any wind hardening during saltation. This not only minimized the influence of particle bonds on particle transport dynamics but provided a plentiful upwind supply of

30   loose snow grains. During this night the streamwise wind direction remained relatively consistent and parallel to the light plane, resulting in a relatively high number of snow particles velocities calculated per frame (up to 50).

Neither neutral stability nor steady-state wind conditions $\left(\frac{\partial U}{\partial t} = 0\right)$ occurred during the field campaign recordings. As $\frac{\partial U}{\partial t} = 0$ is rarely satisfied in the ABL, the less strict steady-state requirements of *Foken and Wichura* (1996) were also tested, further confirming steady-state conditions were not evident. Wind characteristics encompassing three recording times on 23 March are displayed in Table 1. Fifteen minute mean wind speed $\bar{u}$, friction velocity $u_*^2 = \left[\overline{u'w'}^2 + \overline{v'w'}^2\right]^{1/2}$ (*Stull*, 1988),

5 and roughness length $z_0 = z\, e^{-0.4\bar{u}/u_*}$ are shown for anemometer measurements at 40 and 200 cm normal to the snow surface as they are parameters most often used in blowing snow models. However, the ABL did not fit a Prandtl-von Kármán logarithmic-law profile during the storm. Values of $\bar{u}$, u_*, and z_0 over the specific video recording times are also provided in parentheses. Along with turbulence intensity, comparing video recording-averaged (7.3 to 13.1 s) and 15-minute averaged values shows the influence of analysis timescale on characterization of wind flow. Turbulent gust-driven snow transport

10 events dominated the night and these gusts are evident in the video recording timescale averages. However, increasing the timescale from ~10 s to 15-min averaging periods, as is often done in operational models, disguises these turbulent motions. Attempts to relate these values to blowing snow measurements are discussed below.

The wind was characterized by brief moments of intense gusting separated by periods of relatively calm conditions as described in this region by *Helgason and Pomeroy* (2005). Using 15-minute periods to discretize the 23 March observations,

15 90% of the daily total of absolute Reynolds stress ($\tau = |u'w'|$) at 40 cm was generated by events occupying between 39-51% of any given period. For recordings #1, 2 and 3, 90% of total τ was generated by wind occupying 51%, 51%, and 42% of the time, respectively, showing the gusts represented the frequency and magnitude of the winds over the remainder of the night.

3.1 Vertical PTV Profiles

20 Figs. 3a-f show profiles of various aspects of snow particle transport for recordings #1 (Blue), #2 (Green), and #3 (Red), also designated by their recording-specific 40 cm u_* values. Figs. 3a, 3c and 3e show mean u_p at specific heights for ascending particles in the three recordings, with error bars of one standard deviation. Figs. 3b, 3d, and 3f show analogous information for descending particles. Prandtl-von Kármán log-law wind profiles are also displayed in Fig. 3a-f, using the recording specific parameters (u_* and z_0). The alpine wind did not follow a log-linear wind speed profile. This is likely due to the

25 non-neutral, non-stationary and non-steady state nature of the flow as per *Helgason and Pomeroy* (2005) in the same region. The 15-minute roughness lengths generated inaccurate log-linear wind profiles that indicated a zero velocity zone for the wind well above the snow saltation layer. Horizontal dashed lines mark the upper reach of surface microtopography influence on velocity profiles ($z = h_0$), below which erosion and deposition were actively changing the surface structure. The three recordings represent three unique wind events and the resultant snow transport. Following the language of

30 quadrant hole analysis (*Willmarth and Lu*, 1971), Rec #1 is characterized by several strong "ejection" events, where the majority of Reynolds stress is generated by $u' < 0, w' > 0$. These ejections were not accompanied by considerable "sweeps"

$(u' > 0, w' < 0)$ as is often documented in the "bursting process" (*Metzger et al.,* 2010). The wind during Rec #2 consisted of smaller magnitude wind fluctuations around the mean, resulting in the smallest friction velocity of the three recordings. The majority of Reynolds stress is generated by "outward" motions, $u' > 0, w' > 0$. The Reynolds stress of outward motions has opposite sign as ejections, but indicate above average horizontal wind speed fluctuations, which *Sterk et al.* (1998)

5 argued to be of primary importance for aeolian transport. Rec #3 is discussed in detail in section 3.2.

Particle motions begin with an initial ejection velocity at the surface and then accelerate due to fluid drag in the wind. Therefore the height of an ascending saltating particle should be a function of the time spent accelerating. The profiles of horizontal velocities of ascending particles confirm this acceleration in Fig. 3a, 3c, and 3e. The average momentum transfer from wind to grain is estimated from the inverse slope of the plots and indicates the ability of gusty periods to entrain and

10 accelerate particles. For all three recordings there is a near constant particle velocity gradient with height below 10 mm, $\left(\frac{\partial u_p}{\partial z} = \gamma, \gamma \in \mathbb{R}^+ \right)$; above this height, particle velocities are influenced by turbulence. The velocity gradient, γ, was estimated by linear regression as 48.9, 51.6 and 94.0 ms^{-1}/m for recordings #1-3 respectively, and is represented as the inverse slope of the plotted pink lines. These slopes are comparable to wind tunnel PTV sand velocity gradients ($39.0 - 150$ ms^{-1}/m) measured below 30 mm by *Zhang et al.* (2007).

15 The 10 mm transition corresponds with the upper extent of the low-energy population, where transport is characterized by tumbling, very short ballistic hops, and little influence from w'. This is also the region determined by *Creyssels et al.* (2009) and *Ho et al.* (2014) to be largely unaffected by increases in wind speed and is of critical importance for determining bulk flow properties from particle slip and ejection velocities, u_0 and v_0, respectively. While the 10 mm transition height witnessed in the field is lower than that found by *Ho et al.* (2014), this may be due to the increased complexity of natural

20 blowing snow that never achieved saturated equilibrium conditions.

There is qualitative agreement in the shape of ascending and descending snow velocity profiles. However, descending particles show higher velocities and notable deviations from the lines of constant $\frac{\partial u_p}{\partial z}$ after being subjected to longer periods of horizontal acceleration. Figs. 3b, 3d, and 3e profile the fastest moving particles in the lower saltation layer - critical for understanding blowing snow mass flux, surface impact velocities and a complete picture of wind-grain relationships. The

25 difference between descending and ascending velocities, $u_{p\downarrow} - u_{p\uparrow}$, can also been used for determining acceleration rates, and timescales of saltation.

The convex profile of descending u_p is the first PTV evidence suggesting agreement with the log-linear sand PIV/PTV velocity profiles of *Zhang et al.* (2007) for any type of particle in an outdoor environment – its confirmation for snow is particularly interesting. In fact, the sand bed used by *Zhang et al.* (2007) is too short to observe saturated saltation (*Ho et al.*,

30 2014). Thus, the agreement of *Zhang et al.* (2007) with the present study, in contrast to the linearly-varying saturated sand saltation studies of *Creyssels et al.* (2009), may support the importance of determining the domain of application of equilibrium based equations if wind conditions do not allow saturation (i.e. different mechanics of a 'developing' and

'developed' regime of saltation). Higher turbulence intensity in this alpine ABL, intermittent transport and a complex snow surface structure compared to sand make a deeper comparison with the model of *Zhang et al.* (2007) difficult.

The influence of surface microtopography prevents an exact measurement of particle slip velocity u_0, as velocity profiles become unreliable at or immediately above the dashed lines at $z = h_0$ in Fig 3a-f. However, as a first observation, it should
5 be noted that the linear regression plots of constant $du_p/dz = \gamma$ obtain a value of 0.5 m/s for all recordings. It can also seen that $\lim_{z \to h_0^+} u_{p\downarrow}(z) \approx 0.5 \ m/s$ despite intermittent saltation and varying turbulence intensities. This indifference to wind conditions originally conjectured by *Ungar and Haff* (1987) is consistent with several wind tunnel studies (e.g. *Creyssels et al.*, 2009, *Ho et al.* 2014).

The wind conditions during recordings #1 and #2 resulted in similar particle velocity profiles, with comparable
10 maximum u_p (1.5 and 1.6 m/s, respectively) and γ values (48.9 and 51.6 ms^{-1}/m, respectively), but are represented by friction velocities that differ by a factor of 3. Recording #3 is characterized by the fastest particles and largest γ value, though had similar mean wind speeds to recording #1. This difference is proposed to be related to a significant sweep event detailed in section 3.2. The variance of blowing snow particle velocities declines with height, especially below 10 mm for both ascending and descending particles. While there are comparable numbers of high-speed grains above and below 4 mm
15 (discussed later with Fig 3h), the lower variance in particle velocity near the surface corresponds to the large fraction of low-energy grains determining mean velocity in this region; this is characteristic of erodible beds that both absorb and redistribute splash momentum by rebounding high-energy grains but also feed a dense surface flow.

Fig. 3g shows the vertical profile of the fractional particle number flux calculated as Eq. (1):

$$F_z = \frac{n(z) * u_p(z)}{\sum_z \left(n(z) * u_p(z) \right)}, \tag{1}$$

20 where $n(z)$ is the number of particles identified at height z. There is a maximum number flux immediately above the snow surface where u_p is lowest but the particle flow is most dense. Rec #1 ($u_* = 0.26 \ ms^{-1}$) had a noticeably lower height for the number flux maximum because the snow surface was relatively smooth during that recording, with the effects of microtopography dampened. As particle size decreases with height in these flows (e.g. *Sugiura et al.*, 1998; *Gromke et al.*, 2014) the maximum mass flux is likely to be immediately above the snow microtopography as well. Particle number flux
25 maximums at the snow surface appeared in all recordings, over all nights, though how quickly the number density diminished with height appears dependent on instantaneous wind speed (discussed briefly in section 3.2). This is in disagreement with the findings of *Creyssels et al.* (2009) and *Ho et al.* (2012) that characteristic decay height is not dependent on shear stress.

The near surface location of the maximum of F_z is in disagreement with models using Bagnold's focal height (*Bagnold*,
30 1941) to predict a peak mass flux at some distinct height above the surface (e.g. *Pomeroy and Gray,* 1990). This stems from the earlier lack of high resolution measurements of near-snow surface processes outdoors, as results are in agreement with later wind tunnel observations (*Sugiura et al.*, 1998; *Nishimura and Hunt*, 2000) and numerical studies (*Nemoto and*

Nishimura, 2004) of snow flux profiles as well as the recently measured blowing snow density profiles *Gordon and Taylor* (2009) and *Gordon et al.* (2009) found over natural snowcovers in Churchill and Franklin Bay, Canada, respectively.

Projected horizontal velocity histograms for descending particles in Fig. 3h for the near-surface and upper layers of Rec. #3 ($u_* = 0.57\ ms^{-1}$) help illuminate the shift in snow transport mechanics when transitioning to particles in the tail of the particle velocity distributions (*Ho et al.*, 2012). Particle vectors below 1 mm were discarded to eliminate very small velocities from shaking surface particles that do not contribute to the blowing snow flux. Particle velocity vectors within a 4 mm neighborhood of the surface microtopography are in "near-surface region" where a dense flow of short hops dominates. Particles from 4 to 30 mm above the surface determine the "upper layer", where particles capable of splash dominate. Fig. 3h confirms that the near-surface region is dominated by low velocity particles, which are relatively rare in the upper layer. However, the ratio of particles counted in near-surface to the upper regions declines as particle velocity increases, dropping to less than 1 above $u_p = 2\ ms^{-1}$. The dashed line in Fig. 3h displays the difference between the near-surface and upper region histograms. There are 17% more descending particles with velocity $u_p \geq 1.7\ ms^{-1}$ in the upper region compared to the near-surface layer. Because this histogram details only descending particles, the similarity in particle counts implies the near-surface measurements include splashed and tumbling surface gains as well as high-energy particles descending from the upper region.

The area under the difference line constitutes 30% of total particles tracked and 20% of the particle flux, $\sum_z F_z$. These percentages are consistent in other recordings on March 23, as well as recordings over fresh snow on March 5 and 5-day old snow on February 11, with the fraction of total particle flux comprised solely of creep particles ranging from 15 to 25%. Assuming a uniform particle mass distribution, near surface particle motion consumed 22% of the wind kinetic energy transferred to all particles tracked below 30 mm during Rec. #3. Therefore, near-surface measurements have a substantial advantage over typical snow particle counter measurements that are at heights that miss the densest regions of saltation. The lack of consideration of the creep layer as a source of snow saltation flux (*Gauer*, 1999) may be due to the limitations of opto-electronic particle counters when making surface flux measurements. As noted elsewhere (*Creyssels et al.,* 2009), particle-tracking algorithms in the densest regions of saltation are still problematic, and thus these are conservative underestimates of near-surface flux.

The observed histogram shape and convergence were present in all other histograms for 23 March, and during other low wind speed nights, with upper and near surface region particle count convergence velocities varying between 1.2 and 1.7 ms^{-1}. Consistently, near-surface measurements (< 4 mm) appeared to sample the majority of all particle motion below 30 mm. This would have been missed with measurement heights only a few millimeters above. During high wind speed recordings however, this histogram analysis became uncertain because the frame rates limited the fastest particles PTV could track.

3.2 Near-Surface Fluxes

The initiation mechanisms observed at the surface during the onset of transport events differ from those proposed in single threshold velocity models (e.g. *Schmidt*, 1980), suggesting multiple thresholds with the dense surface flow playing a crucial role. All three thresholds recognized during video playback are crossed during recording #3 (Figure 4). Thus, it will be used

5   as an example for further discussion. Concurrent streamwise wind measurements at 200 and 40 cm are plotted in Fig 4a showing penetration of a turbulent sweep to the surface that initiates snow transport. Figs. 4b and 4c show time series of spatially averaged particle velocities, and total particles tracked, respectively, in three height bands, $1 < z < 4\ mm$ (Near-Surface), $4 \le z < 8\ mm$ (Mid), and $8 \le z < 30\ mm$ (High). Fig. 4d shows the time series of the number of pixels occupied by snow crystals in each frame, determined with the *Otsu* (1979) binarization method mentioned above. Pixel area

10   measurements compliment PTV calculations in intense gusting as a snow flux index when individual particle tracking becomes difficult.

At the beginning of the turbulent sweep, snow particle motion began with tumbling surface movement at wind speeds where aerodynamic drag was able to directly break weak crystal bonds and initiate rolling (2.5-5 s in Figs. 4b-d). Particle-bed collisions were concurrently responsible for breaking surface snowpack matrix structures at these wind speeds, though were

15   not yet able to initiate a splash regime. The bonds broken by low-energy grains at low wind speeds enabled more grains to be freely available for entrainment. During this time, horizontal particle velocities remained low and in the near surface region (Fig. 4b), with no particles being tracked above 4mm (Fig 4c), and total mass transport remaining low (minimal pixel area in Fig 4d). At this stage, the only particles in motion were those classically termed creep.

As the wind speed increased, it crossed a threshold above which tumbling near-surface particles were sufficiently accelerated

20   so that they could regularly bounce off the uneven surface and out of the creep layer. This initiated what is classically described as saltation, evidenced by the appearance of particles tracked in the "Mid" and "High" regions in Fig. 4c (above 4 mm), though snow pixel area remained moderate at this time in Fig 4d. As the strongest sweep penetrated to the surface (8.5 s), the last critical wind velocity threshold was crossed; that at which saltating particles are sufficiently accelerated to initiate an active splash regime upon rebounding. At this point the snow particle pixel area signal increased exponentially (Fig. 4d),

25   abruptly saturating the recording frame with snow particles and limiting illumination for successful PTV (discussed below). Similar exponential increases of sand flux during gust onset and splash commencement have been documented (*Willetts et al*., 1991). The role of sweep events such as this for initiating snow saltation are potentially important for developing models that couple turbulence to snow erosion, entrainment and mass flux and may help resolve current uncertainty in estimating threshold conditions for transport. The increased snow pixel area values (Fig 4d) persisted for the duration of the gust, (10 s)

30   after which both high and low streamwise velocities decreased. From 11 s onwards, the decreasing wind speed was no longer able to sustain the mass flux and particles counts dropped in the "Mid" and "High" regions of flow. A combination of inertia and wind drag prolonged transport in the creep layer, maintaining rolling crystals that continued breaking surface bonds and were available for transport during the next gust.

High region particle velocity spikes occurred after 8 s in the PTV time series, but the intense snow particle density blocked the laser light illumination, making particle tracking difficult. At 9 s, the number of particles tracked in the upper region increased as particles tracked near the surface decreased. This is likely a measurement error due to the dense granular flow attenuating light penetration to the snow surface. As the gust subsided, PTV-observed velocities and particle numbers

5   increased because tracking became more successful. Then, as wind speed decreased further, observed velocities and numbers decreased as expected. The *Otsu* (1979) binarization thresholds were determined over short sub-periods of recording #3 (Fig 4d), allowing the thresholding technique to adapt to different levels of illumination and overcome these saturation issues. Analyzing the instantaneous wind signal in Fig. 4a helps explain the source of the fastest moving particles in recording #3. A single turbulent sweep event ($u' > 0, w' < 0$) from 8 to 9 s generated considerable Reynolds stress; this turbulent structure is

10   widely reported to be involved in initiating aeolian sediment transport (*Grass,* 1971; *Jackson*, 1976; *Sterk et al.* 1998; *Chapman et al.,* 2012). This 1 s sweep accounted for 29% and 25% of total absolute Reynolds stress at 40 and 200 cm, respectively, and contributed 56% of total snow particle flux below 30 mm, but only occupied 8% of the time. Turbulent ejections ($u' < 0, w' > 0$) generated 39% of total absolute shear stress during the recording and contributed the same direction of Reynolds stress values to friction velocity calculations but only resulted in 3% of total snow particle flux. This

15   distinction in turbulent sweeps and ejections explains the diminished efficiency of ejections to generate saltation alluded to in section 3.1 with respect to Rec. #1. Varying the lag time between wind and snow measurements from 0 to 1 second to determine the resultant snow flux had no significant effect on these calculations.

In the near-surface region, the ability of the snowpack to redistribute impact kinetic energy was estimated from PTV data derived over the entire measurement season. Snow particle rebound efficiency varied from night to night, and was quantified

20   by the restitution coefficient, $\overline{e_{xz}} = s_r/s_i$, where s_r and s_i are mean ejection and impact speeds of particles in the lowest 3 mm, respectively. Over the course of the campaign, $\overline{e_{xz}}$ varied from 0.61 to 0.85, within the bounds of previous wind tunnel blowing snow studies (*Sugiura and Maeno*, 2000); it remained 0.74 ± 0.04 for all wind speeds on 23 March. This suggests rebound efficiency is dependent on time-sensitive saltating snow crystal and bed mechanical/material properties, as also noted in a wind tunnel study by *McElwaine et al.* (2004).

25   Particle impact dynamics evolved as snowpack surface conditions varied during the season with multiple melt-freeze cycles, periods of wind hardening and the appearance of mixed grain types. Warm (+1°C) February snowstorms precipitated enormous aggregate and rimed crystals that expanded the role of near-surface particle dynamics. Large (4 mm diameter) tumbleweed-like aggregate grains termed here "tumblons", eroded many smaller crystals from the surface or shattered themselves and immediately became saltating grains, depending on impact velocity (Figure 5). This type of particle motion

30   has not been described before and would seem to be a distinctive feature of blowing snow during or shortly after snowfall of large dendritic flakes in relatively warm conditions. Decomposing and aggregate grains of extreme size have not been reported for saltating sand and limit the application of sand bed momentum balances and wind tunnel studies that do not include falling snow to modeling saltating snow in natural conditions.

The Cryosphere

Discussions

Open Access

EGU

4 Discussion

This is the first investigation to measure outdoor snow particle flux and velocity immediately above the snow surface. It provides an opportunity to test certain observations of saltating particle flux trajectories measured in wind tunnels. Though observations were restricted to moderate wind speeds and intermittent transport, they show the importance of creep to

5 blowing snow transport initiation and transition to full saltation. Being able to relate high frequency turbulent wind speed to snow transport (e.g. *Guala et al.*, 2008) is critical in the alpine environment (*Naaim-Bouvet et al.*, 2011) and this study makes a contribution to understanding these dynamics.

From Table 1 and Fig. 3 it is clear that short timescale PTV maximums of u_p, particle velocity gradients $\frac{\partial u_p}{\partial z}$, and flux concentration profiles do not scale with u_{*15} or z_{015} values as is assumed on average for many existing snow saltation

10 models. For example, the highest velocity particles appear with the lowest u_{*15} value (0.28 ms^{-1}) in Fig. 3e-f, evidence of the possible errors occurring when temporally downscaling from mean wind speeds. This reinforces the need to account for variable shear stress in high-resolution modeling (*Doorschot et al.*, 2004; *Groot Zwaaftink et al.*, 2014). Part of this lack of concurrence is due to intermittent transport. The 15-minute mean wind speeds were well below any snow transport thresholds reported in the literature (*Li and Pomeroy*, 1997). The significant errors arising when applying time-averaged

15 values in a u_* driven transport model (i.e. *Bagnold*, 1941) in intermittent winds have been well examined for sand (*Sorenson*, 1997) and equally apply for snow saltation. *Pomeroy and Li* (2000) accounted for the inapplicability of steady state theory in near threshold conditions by using a probability of occurrence function to reduce transport fluxes at lower mean wind speeds, but it is unclear whether this empirical correction can account for the complex interaction of turbulence and particle flux near the threshold. The recording-specific log-law wind profile (Fig 3e-f, solid red line) also underestimated the snow

20 particle speeds during the sweep event observed in Rec. #3. This reinforces the notion that all required assumptions must be met before log-law profiles should be applied (i.e. *George*, 2007).

Steady-state equilibrium saltation models (e.g. *Pomeroy and Gray*, 1990; *Doorschot and Lehning*, 2002) are inappropriate for these situations, with further complications arising from the varying mechanics of transport during gusts, as seen in recording #3. Over short recording periods of less than 10 s, with hundreds of thousands of particle velocity vectors, there

25 are still large standard deviations around mean snow particle velocities (Fig 3). Analysis of recording #3 indicates that there is large variability in snow transport mechanics, with concentration profiles, particle velocities, and saltation height changing over short time scales. This variability appears largely part due to high frequency particle-turbulence interactions and frequent surface impacts.

As mentioned above, 90% of total Reynolds stress at the site was generated over 39-51% of the time on 23 March. In this

30 gusty alpine environment, periodic turbulent gusts generated the majority of momentum flux and $u' > 0$ events disproportionately accounted for snow transport. As suggested by *Sterk et al.* (1998), instantaneous wind speed is a potentially more indicative predictor of snow transport than friction velocity. The importance of understanding snow response to instantaneous wind speed is further increased in complex terrain where the 300 m of clear upwind fetch or 60 s

of constant wind suggested by *Takeuchi* (1980) for saltation to fully develop is not always available. For a more general application, this requires further investigation of turbulent snow transport over longer time series and other snow conditions. Designating creep as distinct from saltation as originally done by *Bagnold* (1941) is not only unnecessary but physically inaccurate as snow transport displays a continuous spectrum of motions, similar to that proposed for sand by *Anders*on

5   (1987), and individual particles can easily transition from one form of motion to another over their trajectories. However, two populations in this spectrum can be delimited by trends in Fig. 3 subplots at $u_p = 1.7 \, ms^{-1}$. In Fig. 3h, $x = 1.7$ coincides with the convergence of upper and lower layer particle count histograms and identifies the high-energy particles descending through both layers. In Fig. 3e, the u_p plot crosses $u_p = 1.7 \, ms^{-1}$ near $z = 10$ mm, the height below which 99% of particles are tracked and above which particle concentrations remain similar with height (Fig 3g). This change in

10   gradient is suspected to correspond with the diminishing frequency of surface impacts and prolonged wind acceleration.

In previous work, 10-20 mm has also corresponded with a transition in flux dynamics exhibited by a change in particle blowing snow density formulae (*Gordon et al.*, 2009) and blowing sand mechanics. Utilizing simultaneous PIV and PTV to obtain two-phase (sand-wind) wind tunnel velocity measurements, *Zhang et al.* (2007) also found a comparable, extremely dense surface flow below this height. Of note, the wind was significantly modified below 15-20 mm in the presence of

15   saltating particles with a shallower convex wind velocity gradient, due to particle momentum extraction in the near-surface region as predicted by Bagnold's focus height (*Bagnold*, 1941). Quantifying transitions that relate particle energy to characteristics of motion and wind response may help to better couple classic saltation models with creep boundary conditions or inform new saltation models that include the full range of initiation mechanism dynamics.

Though the importance of near-surface motions at higher wind speeds in natural conditions remains unclear, the creep layer

20   has proven to be a critical and readily available reservoir of tumbling particles during the onset of saltation. The lower boundary condition for momentum transfer is complex due to creep and dependent on instantaneous wind speed and turbulent motions near the surface. As a result, equilibrium conditions are never achieved. Non-equilibrium saltation-wind interactions cannot be described with simple uniform trajectories. The majority of particle trajectories in saltation consist of short hop lengths and times, resulting in high frequencies of particle collisions that break surface bond structures, and create

25   dense quasi-fluidized bed characteristics. The complexity of conservation of mass, momentum, and kinetic energy in blowing snow in natural environments, such as measured here, cannot be understated, especially when the large rimed, aggregate tumblons are present. In the alpine snowpacks investigated here, highly variable particle restitution coefficients contributed to this complexity, preventing bimodal "erodible" versus "non-erodible" bed descriptions that appear to be viable for sand (*Ho et al.,* 2011).

30   In equilibrium conditions, velocity and flux distributions found in sand studies confirm that the majority of saltation consists of particles tumbling over the surface, and that the properties of flow in the region below twice the Bagnold focus height govern the mean properties of saltating particles (*Creyssels et al.*, 2009; *Ho et al.,* 2011, 2014). This region of particle transport is thus crucial for modeling features of the saltation cloud. Interestingly, sand particle motion in this region was found to be insensitive to increases in mean wind velocity. Presumably, as concentration increases, slip-velocities, u_0, return

to mean values over time. It should be noted that while saturated equilibrium conditions were not found during any of the blowing snow recordings, and near-surface particle velocities reflected instantaneous wind speed fluctuations, u_0 values from snow were comparable to sand u_0 values and were insensitive to changes in mean wind speed. This resiliency may help explain some of the robustness of time-averaged uniform trajectory blowing snow models, but requires further investigation.

5 Despite arguments to the contrary for other materials (e.g. *Sterk et al.*, 1998), saltating snow models relate mass flux to estimated airborne surface shear stress. These estimates are often based on a momentum deficit derived from the total number of particles in transport, neglecting the vertical heterogeneity of particle concentration within the snow saltation layer (*Doorschot and Lehning*, 2002). As all panels in Fig. 3 show, uniform descriptions of surface shear stress calculations based solely on concentration and flux measurements above 10 mm overlook the immense wind momentum transferred into 10 the creep layer (i.e. *Zhang et al.,* 2007, *Creyssels et al.,* 2009; *Ho et al.,* 2011, 2012, 2014). Disregarding this flux prevents calculation of an accurate momentum balance. Accounting for variability in saltation trajectories would also allow for a dense surface flow to be represented that can feed upper regions (e.g. *Nemoto and Nishimura*, 2004) and create a self-consistent momentum balance. *Andreotti* (2004) wrote a further discussion of self-consistency errors of wind feedback in single trajectory saltation models.

15 The wide variety of snow saltation initiation mechanisms observed in this experiment is in contrast to classic initiation models that assume that a temporally-constant fraction of saltating grains begin motion through either aerodynamic entrainment or splash (e.g. *Pomeroy and Gray*, (1990)). As seen in Fig 4, in intermittent conditions this variability is magnified, as splash regimes themselves are intermittent, depending on sufficient wind speed for adequate particle acceleration upon ejection from the snow surface. It could be very useful to compare modeled entrainment and splash ratios 20 with PTV datasets, however longer recording times over a larger variety of snow types would be necessary to obtain statistically significant comparisons. Specifically, whether long time average statistics can account for periods of varying initiation during intermittent saltation, or only can apply in more nearly steady-state environments would be a useful finding for high temporal resolution applications (e.g. *Groot Zwaaftink et al.*, 2014).

5 Conclusion

25 The first environmental PTV computations for blowing snow have proven to be a viable avenue for exploring complex wind-snow interactions at millisecond timescales in natural, non-steady state, high Reynolds number wind conditions. These results support the need for further conceptual advancement of models of snow saltation, initiation and rebound, including multiple types of motion and the interaction of turbulent sweeps on particle erosion and entrainment. Over short timescales, snow particle behaviour is influenced by complex wind speed dependent initiation and rebound dynamics, including a 30 variable dense surface flow that is beyond the scope of scalar aerodynamic entrainment and splash parameterizations. The wind-to-snow and snow-to-snow momentum transfer in the first few millimeters above the surface is critical for both driving mechanisms of transport initiation as well as providing lower boundary conditions for two-phase atmospheric flows.

The Cryosphere
Discussions

Open Access

EGU

A spectrum of particle motion was found in the majority of recordings. Sand saltation velocity distribution models do not comprehensively describe transport of complex snow crystal structures such as the previously undescribed tumblon motions or snow particle shattering and sintering. Near-surface particles below 10 mm contribute considerably to saltation by both bouncing into upper saltation regions and by breaking snow bed matrix bonds, making particles freely available for splash

5 and entrainment with reduced wind drag requirements.

The ability of the snowpack surface to absorb wind and particle momentum in the dense surface region of saltation appears variable and substantial. The near-surface layer was observed to be the region of peak snow particle concentration. In the wind conditions investigated, this high particle concentration compensated for the reduced particle speeds near the surface, and sustained a layer of peak particle and likely mass flux. The creep layer has far more intricate dynamics and greater flux

10 relevance than previously described, and is a dynamic zone of erosion and deposition during snow transport whilst feeding the saltation layer immediately above. Saltation dynamics are therefore dependent upon creep particle motions, which mediate exchange between the snow surface and blowing snow.

Snow saltation velocities, heights, and particle concentrations responded on scales of < 1 s to turbulent wind speed fluctuations. Analysis of a turbulent sweep event has shown that snow transport is sensitive to different generators of

15 Reynolds stress. PTV shows potential to answer many open questions in blowing snow research through quantification of momentum redistribution in very near-surface particle motion. The use of high temporal-resolution outdoor PTV measurements may prove useful in future work for understanding the turbulent influences on intermittent blowing snow processes and allows comparison with and evaluation of wind tunnel PTV data.

6. ACKNOWLEDGEMENTS

References

25 Anderson, R. S. and Haff, P. K.: Simulation of eolian saltation., Science, 241(4867), 820–3, doi:10.1126/science.241.4867.820, 1988.

Anderson, R. S.: Eolian Sediment Transport as a Stochastic Process: The Effects of a Fluctuating Wind on Particle Trajectories, J. Geol., 95(4), 497–512, doi:10.1086/629145, 1987.

Andreotti, B.: A two species model of aeolian sand transport, J. Fluid Mech., 510, 47–70, 2004.

30 Bagnold, R. A.: The Physics of Blown Sand and Desert Dunes, 1st ed., Methuen & Co. Limited, London., 1941.

The Cryosphere
Discussions
Open Access
EGU

Bintanja, R.: Snowdrift suspension and atmospheric turbulence. Part I: Theoretical background and model description, Boundary-layer Meteorol., 95, 343–368, 2000.

Brown, T. and Pomeroy, J.: A blowing snow particle detector, Cold Reg. Sci. Technol., 16, 167–174, 1989.

Budd, W. F., Dingle, W. R. J. and Radok, U.: The Byrd snow drift project: Outline and basic results, in Studies in Antarctic

5 Meteorology, edited by M. J. Rubin, pp. 59–70, American Geophysical Union, Washington D.C., 1966.

Chapman, C. a., Walker, I. J., Hesp, P. a., Bauer, B. O. and Davidson-Arnott, R. G. D.: Turbulent Reynolds stress and quadrant event activity in wind flow over a coastal foredune, Geomorphology, 151-152, 1–12, doi:10.1016/j.geomorph.2011.11.015, 2012.

Creyssels, M., Dupont, P., El Moctar, a. O., Valance, A., Cantat, I., Jenkins, J. T., Pasini, J. M. and Rasmussen, K. R.:

10 Saltating particles in a turbulent boundary layer: experiment and theory, J. Fluid Mech., 625, 47–74, doi:10.1017/S0022112008005491, 2009.

Doorschot, J., Lehning, M. and Vrouwe, A.: Field measurements of snow-drift threshold and mass fluxes, and related model simulations, Boundary-Layer Meteorol., 347–368, 2004.

Doorschot, J. J. J. and Lehning, M.: Equilibrium saltation: mass fluxes, aerodynamic entrainment, and dependence on grain

15 properties, Boundary-layer Meteorol., 104, 111–130, 2002.

Dyunin, A. K. and Kotlyakov, V.: Redistribution of snow in the mountains under the effect of heavy snow-storms, Cold Reg. Sci. Technol., 3, 287–294, 1980.

Fierz, C., Armstrong, R., Durand, Y., Etchevers, P., Greene, E., McClung, D. M., Nishimura, K., Satyawali, P. K. and Sokratov, S. A.: The international classification for seasonal snow on the ground, International Association of Cryospheric

20 Sciences., 2009.

Foken, T. and Wichura, B.: Tools for quality assessment of surface-based flux measurements, Agric. For. Meteorol., 78, 83–105, doi:10.1016/0168-1923(95)02248-1, 1996.

Gauer, P.: Blowing and Drifting Snow in Alpine Terrain: A Physically-Based Numerical Model and Related Field Measurements, Swiss Federal Institute of Technology Zurich., 1999.

25 George, W. K.: Is there a universal log law for turbulent wall-bounded flows?, Philos. Trans. A. Math. Phys. Eng. Sci., 365(1852), 789–806, doi:10.1098/rsta.2006.1941, 2007.

Gordon, M., Savelyev, S. and Taylor, P. a.: Measurements of blowing snow, part II: Mass and number density profiles and saltation height at Franklin Bay, NWT, Canada, Cold Reg. Sci. Technol., 55(1), 75–85, doi:10.1016/j.coldregions.2008.07.001, 2009.

30 Gordon, M. and Taylor, P. a.: Measurements of blowing snow, Part I: Particle shape, size distribution, velocity, and number flux at Churchill, Manitoba, Canada, Cold Reg. Sci. Technol., 55(1), 63–74, doi:10.1016/j.coldregions.2008.05.001, 2009.

Gromke, C., Horender, S., Walter, B. and Lehning, M.: Snow particle characteristics in the saltation layer, J. Glaciol., 60(221), 431–439, doi:10.3189/2014JoG13J079, 2014.

Groot Zwaaftink, C. D., Diebold, M., Horender, S., Overney, J., Lieberherr, G., Parlange, M. B. and Lehning, M.: Modelling Small-Scale Drifting Snow with a Lagrangian Stochastic Model Based on Large-Eddy Simulations, Boundary-Layer Meteorol., doi:10.1007/s10546-014-9934-2, 2014.

Guala, M., Manes, C., Clifton, a. and Lehning, M.: On the saltation of fresh snow in a wind tunnel: Profile characterization and single particle statistics, J. Geophys. Res. Earth Surf., 113(3), 1–13, doi:10.1029/2007JF000975, 2008.

Helgason, W. and Pomeroy, J.: Uncertainties in estimating turbulent fluxes to melting snow in a mountain clearing, in Proc. 62nd Eastern Snow Conf, pp. 129–142., 2005.

Ho, T. D., Dupont, P., Ould El Moctar, A. and Valance, A.: Particle velocity distribution in saltation transport, Phys. Rev. E - Stat. Nonlinear, Soft Matter Phys., 85(5), 1–5, doi:10.1103/PhysRevE.85.052301, 2012.

Ho, T. D., Valance, A., Dupont, P. and Ould El Moctar, A.: Aeolian sand transport: Length and height distributions of saltation trajectories, Aeolian Res., 12, 65–74, doi:10.1016/j.aeolia.2013.11.004, 2014.

Ho, T. D., Valance, A., Dupont, P. and Ould El Moctar, A.: Scaling laws in aeolian sand transport, Phys. Rev. Lett., 106(9), 4–7, doi:10.1103/PhysRevLett.106.094501, 2011.

Jackson, R. G.: Sedimentological and fluid-dynamic implications of the turbulent bursting phenomenon in geophysical flows, J. Fluid Mech., 77(03), 531, doi:10.1017/S0022112076002243, 1976.

Kinar, N. J. and Pomeroy, J. W.: Measurement of the physical properties of the snowpack, Rev. Geophys., 53, doi:10.1002/2015RG000481.Received, 2015.

Kobayashi, D.: Studies of Snow Transport in Low-Level Drifting Snow, Sapporo, Hokkaido, Japan., 1972.

Li, B. and McKenna Neuman, C.: Boundary-layer turbulence characteristics during aeolian saltation, Geophys. Res. Lett., 39(11), 1–6, doi:10.1029/2012GL052234, 2012.

Li, L. and Pomeroy, J. W.: Estimates of Threshold Wind Speeds for Snow Transport Using Meteorological Data, J. Appl. Meteorol., 36, 205–213, 1997.Lü, X., Huang, N. and Tong, D.: Wind tunnel experiments on natural snow drift, Sci. China Technol. Sci., 55(4), 927–938, doi:10.1007/s11431-011-4731-3, 2012.

Mcelwaine, J. N., Maeno, N. and Sugiura, K.: The Splash Function for Snow From Wind-Tunnel Measurements, Ann. Glaciol., 38, 71–78, 2004.

Morris, S. C., Stolpa, S. R., Slaboch, P. E. and Klewicki, J. C.: Near-surface particle image velocimetry measurements in a transitionally rough-wall atmospheric boundary layer, J. Fluid Mech., 580, 319–338, doi:10.1017/S0022112007005435, 2007.

Naaim-Bouvet, F., Naaim, M., Bellot, H. and Nishimura, K.: Wind and drifting-snow gust factor in an Alpine context, Ann. Glaciol., 52(58), 223–230, doi:10.3189/172756411797252112, 2011.

Nemoto, M. and Nishimura, K.: Numerical simulation of snow saltation and suspension in a turbulent boundary layer, J. Geophys. Res., 109(D18), -, doi:10.1029/2004JD004657, 2004.

Nishimura, K. and Hunt, J. C. R.: Saltation and incipient suspension above a flat particle bed below a turbulent boundary layer, J. Fluid Mech., 417, 77–102, doi:10.1017/S0022112000001014, 2000.

The Cryosphere
Discussions

Open Access

EGU

Nishimura, K., Yokoyama, C., Ito, Y., Nemoto, M., Naaim-bouvet, F., Bellot, H., Fujita, K., Yokoyama, C., Ito, Y., Nemoto, M., Naaim-bouvet, F., Bellot, H. and Fujita, K.: Snow particle speeds in drifting snow, J. Geophys. Res. Atmos., 119, 9901–9913, doi:10.1002/2014JD021686, 2014.

Otsu, N.: A Threshold Selection Method from Gray-Level Histograms, IEEE Trans. Syst. Man. Cybern., SMC-9(1), 62–66, 5   1979.

Owen, P. R.: Saltation of uniform grains in air, J. Fluid Mech., 20(02), 225, doi:10.1017/S0022112064001173, 1964.

Pomeroy, J. W. and Male, D. H.: Steady-state suspension of snow, J. Hydrol., 136(1-4), 275–301, doi:10.1016/0022-1694(92)90015-N, 1992.Pomeroy, J. W. and Gray, D. M.: Snowcover: Acumulation, Relocation, and Management, Saskatoon, SK., 1995.

10   Pomeroy, J., Fang, X. and Ellis, C.: Sensitivity of snowmelt hydrology in Marmot Creek, Alberta, to forest cover disturbance, Hydrol. Process., 26(12), 1891–1904, doi:10.1002/hyp.9248, 2012.

Pomeroy, J. and Gray, D.: Saltation of snow, Water Resour. Res., 26(7), 1583–1594, 1990.

Pomeroy, J. and Li, L.: Prairie and Arctic areal snow cover mass balance using a blowing snow model, J. Geophys. Res. …, 105(D21), 26619–26634, 2000.

15   Rosi, G. a., Sherry, M., Kinzel, M. and Rival, D. E.: Characterizing the lower log region of the atmospheric surface layer via large-scale particle tracking velocimetry, Exp. Fluids, 55(5), 10, doi:10.1007/s00348-014-1736-2, 2014.

Schmidt, R. A.: Measuring Particle Size and Snowfall Intensity in Drifting Snow, Cold Reg. Sci. Technol., 9, 121–129, 1984.

Schmidt, R. A.: Properties of blowing snow, Rev. Geophys., 20(1), 39–44, 1982.

20   Schmidt, R. A.: Threshold Wind-Speeds and Elastic Impact in Snow Transport, J. Glaciol., 26(94), 453–467, 1980.

Schweizer, J., Jamieson, B. and Schneebeli, M.: Snow avalanche formation, Rev. Geophys., 41(4), doi:10.1029/2002RG000123, 2003.

Sørensen, M.: On the effect of time variability of the wind on rates of aeolian sand transport, Aarhus Geosci., 7, 73–77, 1997.

25   Sterk, G., Jacobs, a. F. G. and Van Boxel, J. H.: The effect of turbulent flow structures on saltation sand transport in the atmospheric boundary layer, Earth Surf. Process. Landforms, 23(10), 877–887, doi:10.1002/(SICI)1096-9837(199810)23:10<877::AID-ESP905>3.0.CO;2-R, 1998.

Stull, R.: An Introduction to Boundary layer Meteorology, Kluwer Academic Publisher, Dordrecht, The Netherlands.,1988.

Sugiura, K. and Maeno, N.: Wind-tunnel measurements of restitution coefficients and ejection number of snow particles in 30   drifting snow: determination of splash functions, Boundary-Layer Meteorol., 95(1), 123–143, 2000.

Sugiura, K., Nishimura, K., Maeno, N. and Kimura, T.: Measurements of snow mass flux and transport rate at different particle diameters in drifting snow, Cold Reg. Sci. Technol., 27(2), 83–89, doi:10.1016/S0165-232X(98)00002-0, 1998.

Tabler, R. D.: Snow Transport as a Function of Wind Seep and Height, in Proceedings, Cold Regions Sixth International Specialty Conference TCCP/ASCE, pp. 729–738, Cold Regions Engineering, West Lebanon, NH., 1991.

Takeuchi, M.: Vertical Profile and Horizontal Increase of Drift-Snow Transport, J. Glaciol., 26(94), 481–492, 1980.

Toloui, M., Riley, S., Hong, J., Howard, K., Chamorro, L. P., Guala, M. and Tucker, J.: Measurement of atmospheric boundary layer based on super-large-scale particle image velocimetry using natural snowfall, Exp. Fluids, 55(5), 14, doi:10.1007/s00348-014-1737-1, 2014.

5   Tominaga, Y., Okaze, T., Mochida, A., Sasaki, Y., Nemoto, M. and Sato, T.: PIV measurements of saltating snow particle velocity in a boundary layer developed in a wind tunnel, J. Vis., 16(2), 95–98, doi:10.1007/s12650-012-0156-8, 2012.

Ungar, J. E. and Haff, P. K.: Steady state saltation in air, Sedimentology, 34(2), 289–299, doi:10.1111/j.1365-3091.1987.tb00778.x, 1987.

Vickers, D. and Mahrt, L.: Quality control and flux sampling problems for tower and aircraft data, J. Atmos. Ocean.
10   Technol., 14(3), 512–526, doi:10.1175/1520-0426(1997)014<0512:QCAFSP>2.0.CO;2, 1997.

Willetts, B. B., McEwan, J. and Rice, M. A.: Initiation of motion of quartz sand grains, Acta Mech., 1, 123–134, 1991.

Willmarth, W. W. and Lu, S. S.: Structure of the Reynolds stress near the wall, J. Fluid Mech., 55(1), 65–92, doi:10.1017/S002211207200165X, 1972.

Winstral, A., Marks, D. and Gurney, R.: Simulating wind-affected snow accumulations at catchment to basin scales, Adv.
15   Water Resour., 55, 64–79, doi:10.1016/j.advwatres.2012.08.011, 2013.

Zhang, W., Wang, Y. and Lee, S. J.: Two-phase measurements of wind and saltating sand in an atmospheric boundary layer, Geomorphology, 88(1-2), 109–119, doi:10.1016/j.geomorph.2006.10.017, 2007.

Zhu, W., van Hout, R. and Katz, J.: PIV Measurements in the Atmospheric Boundary Layer within and above a Mature Corn Canopy. Part II: Quadrant-Hole Analysis, J. Atmos. Sci., 64(8), 2825–2838, doi:10.1175/JAS3990.1, 2007.
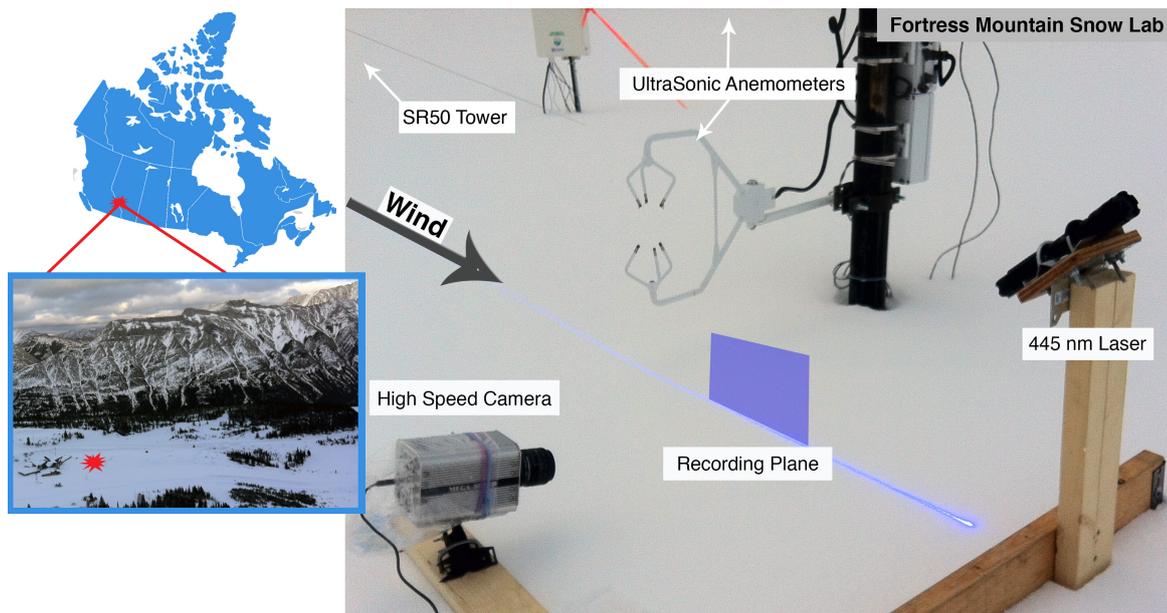
20

Figure 1: Blowing snow instrument setup and location of field site, Fortress Mountain Snow Laboratory, Alberta, Canada
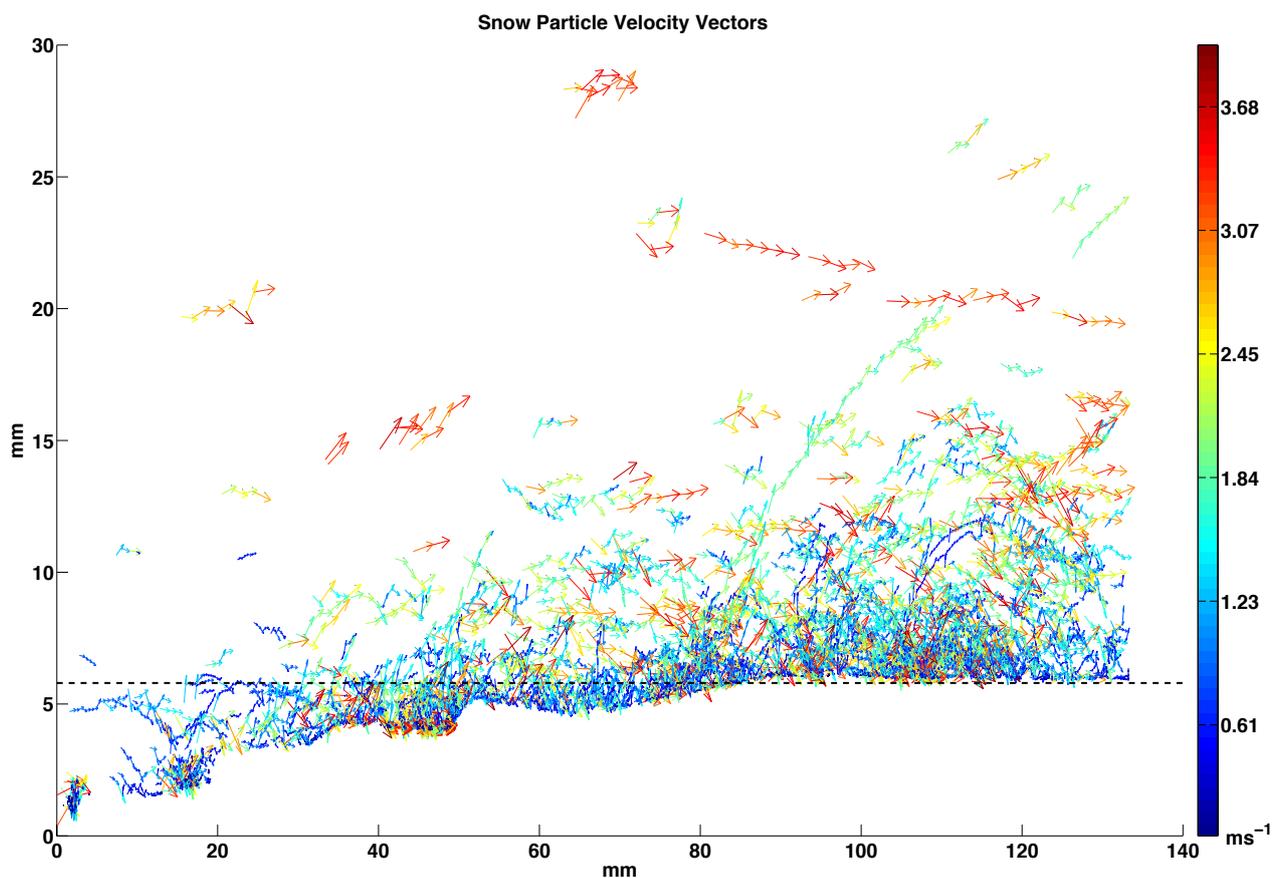
5

Figure 2: Sparse snow particle velocity vector field during one second of recording on 23 March, vector colors scaled according to total particle speed. The dashed line shows reference below which particles are influenced by microtopography.
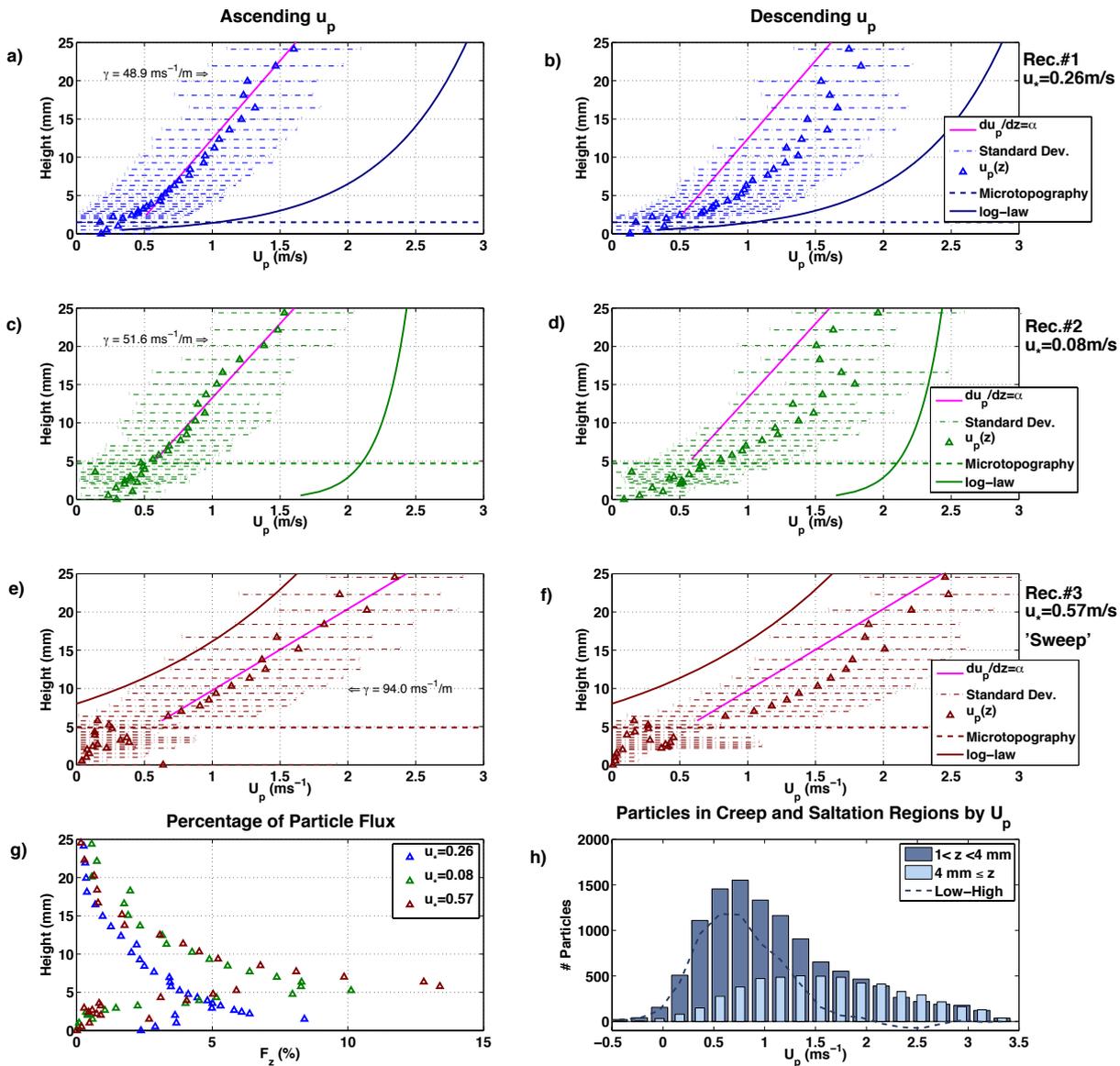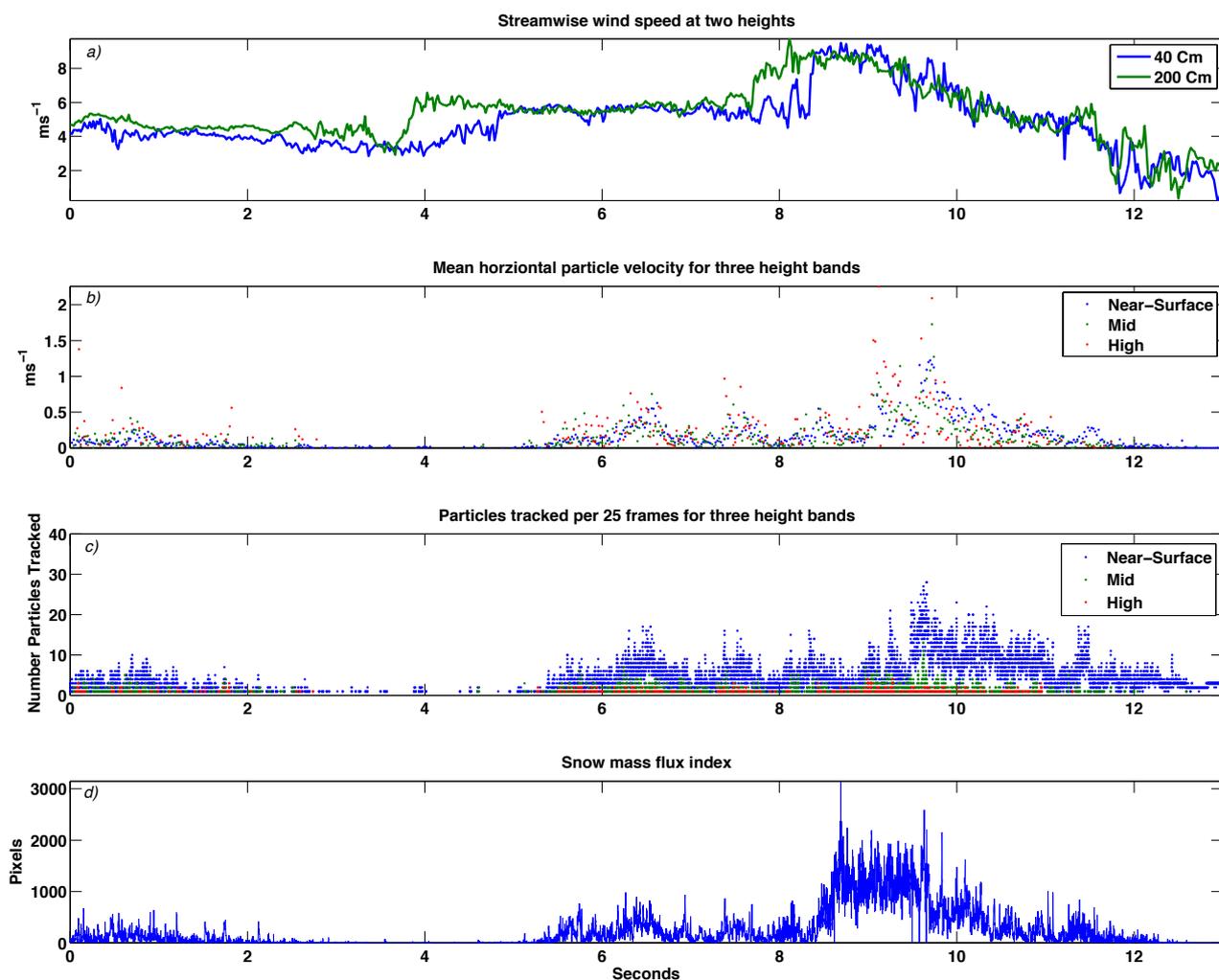
Figure 3 a-f): Ascending and descending mean snow particle horizontal velocity profiles (u_p), with one standard deviation error bars, log-law wind profiles for recording specific values (solid lines), and plots of constant $du_p/dz = \gamma$. 3g) Particle number flux concentration profiles, 3h) Descending snow particle velocity histograms for two height bands for the $u_* = 0.57\ ms^{-1}$ recording on March 23, 2015.

Figure 4: 23 March, recording #3 time series. a) 50Hz streamwise wind speed at 40 and 200 cm above snow surface. b) 50 Hz Snow particle velocities obtained by binning particle vectors in three height bands (1<z<4 mm (Near-Surface), 4<z<8 mm (Mid), 8<z<30 mm (High)), then temporally averaging. c) Number of tracked particles in same height bands per frame (1250 Hz), d) *Otsu* (1979) binarization snow particle pixel area per frame (1250 Hz).
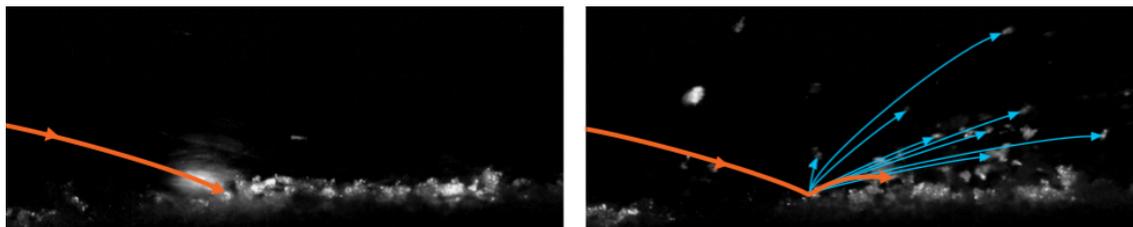
Figure 5. Splash and inbound Tumblon collapse. Timestep 11.4 ms, Feb 5, 2015

5

The Cryosphere
Discussions

Open Access

EGU

Recording	Duration/Frames	$\bar{u}$ m s^{-1}	u_* m s^{-1}	z_0 mm	Turb. Int.
#1	7.3 s/9147				
200 cm		1.2 (5.5)	0.61 (0.23)	910.1 (0.1)	1.10 (0.22)
40 cm		1.1 (4.7)	0.46 (0.26)	126.9 (0.3)	1.13 (0.27)
#2	11.4 s/14299				
200 cm		1.9 (4.3)	0.48 (0.22)	410.6 (0.8)	1.04 (0.24)
40 cm		1.7 (4.2)	0.40 (0.08)	69.9 (1.3 e-4)	1.04 (0.16)
#3	13.1 s/16404				
200 cm		1.4 (5.3)	0.28 (0.55)	312.2 (42.4)	0.80 (0.40)
40 cm		1.3 (4.8)	0.24 (0.57)	116.5 (8.0)	0.79 (0.45)

Table 1: Wind characteristics: mean wind speed, friction velocity, aerodynamic roughness height and turbulent intensity for recordings #1-3 on the evening of Mar. 23, 2015. Average values from the 15 minutes surrounding each recording (and recording-only period in parentheses) are shown for the two measurement heights